Original Article

Quantitative parameters of contrast-enhanced ultrasound effectively promote the prediction of cervical lymph node metastasis in papillary thyroid carcinoma

Biao Su[1,2,§], Lisha Li[3,4,§], Yingchun Liu[1,§], Hui Liu[1,5], Jia Zhan[1], Qiliang Chai[1], Liang Fang[1], Ling Wang[3,4,*], Lin Chen[1,*]

[1] Department of Ultrasound, Huadong Hospital, Fudan University, Shanghai, China;
[2] Department of Ultrasound, Shuguang Hospital, Shanghai University of Traditional Chinese Medicine, Shanghai, China;
[3] Department of Reproductive Immunology, Obstetrics and Gynecology Hospital, Fudan University, Shanghai, China;
[4] Shanghai Key Laboratory of Clinical Geriatric Medicine, Shanghai, China;
[5] Department of Ultrasound, Shanghai Cancer Center, Fudan University, Shanghai, China.

SUMMARY   Papillary thyroid carcinoma (PTC), the most common endocrine tumor, often spreads to cervical lymph nodes metastasis (CLNM). Preoperative diagnosis of CLNM is important when selecting surgical strategies. Therefore, we aimed to explore the effectiveness of quantitative parameters of contrast-enhanced ultrasound (CEUS) in predicting CLNM in PTC. We retrospectively analyzed 193 patients with PTC undergoing conventional ultrasound (CUS) and CEUS. The CUS features and quantitative parameters of CEUS were evaluated according to PTC size ≤ 10 or > 10 mm, using pathology as the gold standard. For the PTC ≤ 10 mm, microcalcification and multifocality were significantly different between the CLNM (+) and CLNM (-) groups (both $P < 0.05$). For the PTC > 10 mm, statistical significance was noted between the two groups with respect to the margin, capsule contact, and multifocality (all $P < 0.05$). For PTC ≤ 10 mm, there was no significant difference between the CLNM (+) and CLNM (-) groups in all quantitative parameters of CEUS (all $P > 0.05$). However, for PTC > 10 mm, the peak intensity (PI), mean transit time, and slope were significantly associated with CLNM (all $P < 0.05$). Multivariate analysis showed that PI > 5.8 dB was an independent risk factor for predicting CLNM in patients with PTC > 10 mm ($P < 0.05$). The area under the curve of PI combined with CUS (0.831) was significantly higher than that of CUS (0.707) or PI (0.703) alone in the receiver operator characteristic curve analysis ($P < 0.05$). In conclusion, PI has significance in predicting CLNM for PTC > 10 mm; however, it is not helpful for PTC ≤ 10 mm.

Keywords   contrast-enhanced ultrasound, quantitative parameter, papillary thyroid carcinoma, cervical lymph node metastasis

1. Introduction

Papillary thyroid carcinoma (PTC) accounts for approximately 80% of all malignant thyroid tumors, and its incidence has increased in recent decades (*1-3*). Although, as compared to other cancers, most PTC demonstrate benign behavior and have a better prognosis after surgery, the occurrence of cervical lymph node metastasis (CLNM) contributes to a poor prognosis, including local recurrence, distant metastasis, and even death (*4,5*). PTC has a high rate of CLNM, ranging from 20% to 90% (*6,7*). CLNM commonly occurs first in the central region of the neck (*8*). According to the revised American Thyroid Association guidelines, PTC patients

should undergo preventive central lymph node dissection (CLND) (*9*). However, prophylactic CLND increases the extent of surgery, temporary laryngeal nerve injury, and other complications (*10-12*). The effectiveness versus risk of central lymph node dissection remains controversial when complications after surgery are considered.

Some studies have reported an association between tumor size and CLNM (*7,13,14*). However, the risk factors for CLNM correlating with the size of the PTC are not always consistent. Li *et al.* (*15*) reported that PTC > 10 mm correlated with CLNM, whereas in a multivariate analysis, Chen *et al.* (*16*) found that PTC size was not associated with CLNM. Conventional

ultrasound (CUS) is the first imaging method used to assess CLNM and preoperatively stage patients with PTC to determine the extent of surgery. However, CUS can detect only 20%–31% of PTC patients with central neck lymph node metastasis (*17*). Contrast-enhanced ultrasound (CEUS) with sensitive detection of tissue blood perfusion has been used to differentiate malignant from benign thyroid nodules (*18-20*). To our knowledge, some researchers have focused on the ability of CEUS to predict CLNM in patients with PTC using qualitative or quantitative analysis, and the value remains controversial owing to discrepant results or different methodologies (*21,22*).

Therefore, this study mainly focuses on the CEUS characteristics of PTC to identify appropriate quantitative parameters and the best cutoff value to predict CLNM according to the nodule size.

2. Materials and Methods

2.1. Patients

Between August 2019 and March 2021, 268 PTC in 268 patients underwent CEUS after a CUS examination. The inclusion criteria were as follows: (1) patients who had undergone total or near-total thyroidectomy combined with neck lymph node dissection; and (2) thyroid nodules confirmed as PTC by histopathological examination. The exclusion criteria were as follows: (1) patients who had not undergone neck lymph node dissection; and (2) insufficient CUS and CEUS images of the thyroid nodules for analysis. Of the 268 patients, 46 (17.2%) were excluded because of the absence of neck lymph node dissection, 11 (4.1%) because of incomplete CUS documents, and 18 (6.7%) because of incomplete CEUS images. Thus, 193 patients (101 women and 92 men) with confirmed PTC were included. Among the 193 patients with PTC, 79 had CLNM and 114 did not. The thyroid nodule size ranged from 2 to 58 mm (9.8 ± 6.7mm). The patient's age ranged from 22-74 years (45.6 ± 12.6 years). Figure 1 depicts the flowchart of the 193 patients selected.

This study was approved by the Institutional Review Board and Ethics Committee of Fudan University and conducted in accordance with the Declaration of Helsinki. Each patient signed an informed consent form prior to the ultrasound examination.

2.2. CUS and CEUS examinations

All thyroid lesions were examined by a sonographer (L.C.) with more than 10 years of experience in CUS and CEUS. An Aplio500 system (Toshiba Medical Systems Corp., Tokyo, Japan) with a 5-14 MHz linear transducer was used. Grayscale ultrasound and CDFI were performed for each thyroid nodule to assess nodule morphology and blood flow characteristics. The largest dimension of the nodule on CUS was measured and its size documented. CEUS examination was performed after CUS using the Aplio500 system at a low
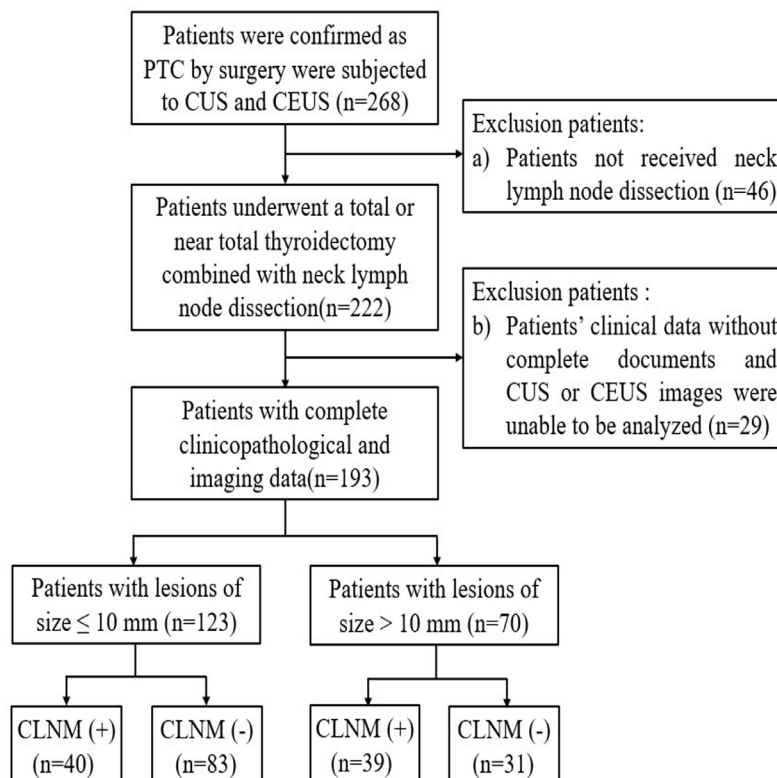

Figure 1. Flowchart of study participants included and excluded in the study.

mechanical index of 0.05-0.10. The contrast agent used in this study, SonoVue, is composed of microbubbles filled with sulfur hexafluoride (SF6) and phospholipids. For this, 5 mg of SonoVue was mixed with 5 mL 0.9% physiological saline and gently shaken to create a microbubble suspension. The SonoVue suspension (1.2 mL) was injected as a bolus, followed by an immediate rinse with 5 mL saline. At the same time, the timer and recording software were started, the imaging lasted at least 2 min, and the images were stored in digital form.

2.3. Image review and data evaluation

The CUS and CEUS characteristics of the thyroid nodules were reviewed by two radiologists (B.S. and Y.C.L.), who were blinded to the patient identities and pathological results. The CUS characteristics of thyroid nodules that were documented and described included location (lower, upper, middle, or isthmus), echogenicity (iso/hyperechoic, hypoechoic, or markedly hypoechoic), margin (regular or irregular), composition (mixed or solid), shape (wider than tall, taller than wide), microcalcification (present or absent), halo sign (present or absent), capsule contact (present or absent), diffuse lesion (present or absent), multifocality (present or absent), and blood flow signal on CDFI (avascularity, peripheral vascularity, central vascularity, or mixed vascularity). Multifocality was defined as the presence of multiple lesions discovered on ultrasonography and confirmed by pathology. Time-intensity curve (TIC) analysis software was used to obtain quantitative parameters. The following quantitative parameters were obtained from the TIC of CEUS: (1) peak intensity (PI, in dB): the intensity corresponding to the highest point on the curve; (2) time to peak (TTP, in seconds): the time from the origin to the point of PI; (3) mean transit time (MTT, in seconds): the time of intensity dropped from peak to 50% on the curve; (4) slope (SL, in dB/s): the slope coefficient of the ascent curve; (5) area under the curve (AUC, dB.s): the area under the entire curve; (6) area wash in (AWI, dB.s): the area under the ascending portion of the curve; and (7) area wash out (AWO, dB.s): the area under the decreasing portion of the curve.

Based on the images, the two radiologists made the final conclusion. If there were differences in the evaluation of specific thyroid images, a final consensus was reached through mutual consultation.

2.4. Statistical analysis

Continuous quantitative data was represented by the mean ± standard deviation and compared with the independent-sample t test. The χ^2 test and Fisher's exact tests were employed for discrete variables that were represented by numbers and percentages. Multivariate logistic regression analysis was used to identify the independent predictors of CLNM in patients with PTC. A receiver operating characteristic (ROC) curve was constructed to determine AUC, sensitivity, and specificity. Differences between the various methods were compared using the Z-test. Statistical Product and Service Solutions (SPSS) 25.0, and MedCalc Statistics version 19.6 were used for the statistical analysis. $P < 0.05$ was considered statistically significant.

3. Results

3.1. Baseline characteristics and pathological findings

Of the 193 PTC, 123 (63.7%) were ≤ 10 mm, 40 (20.7%) were CLNM (+), 83 (43.0%) were CLNM (-), 70 (36.3%) were > 10 mm, 39 (20.2%) were CLNM (+), and 31 (16.1%) were CLNM (-). For the PTC ≤ 10 mm, significant differences between the CLNM (+) and CLNM (-) groups were noted with respect to size and age (both $P < 0.05$). In contrast, for PTC > 10 mm, there was only a significant difference in size between the CLNM (+) and CLNM (-) groups ($P < 0.05$). As regards the sex and location for PTC ≤ 10 mm and the age, sex, and location for PTC > 10 mm, the proportion of the CLNM (-) groups was similar to the CLNM (+) groups ($P > 0.05$ for all) (Table 1).

3.2. CUS features

For the PTC ≤ 10 mm on CUS, the microcalcification

Table 1. Baseline characteristics and pathological findings

Characteristics	≤ 10 mm (n = 123)		P	> 10 mm (n = 70)		P
	CLNM (-) (n = 83)	CLNM (+) (n = 40)		CLNM (-) (n = 31)	CLNM (+) (n = 39)	
Size	5.9 ± 1.8	7.0 ± 1.9	0.002	12.9 ± 4.4	18.9 ± 8.9	0.000
Mean age	48.0 ± 11.6	41.9 ± 13.3	0.010	47.3 ± 12.2	42.2 ± 14.3	0.119
Sex			0.239			0.851
Male	34 (27.6)	12 (9.8)		20 (28.6)	26 (37.1)	
Female	49 (39.8)	28 (22.8)		11 (15.7)	13 (18.6)	
Multifocal			0.019			0.037
Absent	63 (51.2)	22 (17.9)		22 (31.4)	18 (25.7)	
Present	20 (16.3)	18 (14.6)		9 (12.9)	21 (30.0)	

CLNM, cervical lymph node metastasis; PTC, papillary thyroid carcinoma; Values are presented as the number (%).

and multifocality were significantly different between the CLNM (+) and CLNM (-) groups (*P* = 0.000 and 0.019, respectively). There was no statistical significance between the two groups in terms of composition, echogenicity, shape, margin, halo sign, capsule contact, diffuse lesion, and CDFI pattern (*P* > 0.05 for all). However, for PTC > 10 mm, statistically significant differences were noted between the CLNM (+) and CLNM (-) groups in terms of margin, capsule contact, and multifocality on CUS (*P* = 0.024, 0.030, and 0.037, respectively). No significant difference was noted between the groups in terms of the composition, echogenicity, shape, microcalcification, halo sign, diffuse lesion, multifocality, and CDFI patterns (*P* > 0.05 for all) (Figure 2). Table 2 details the CUS features of the CLNM (+) and CLNM (-) groups for PTC ≤ 10 mm and PTC > 10 mm.

3.3. Quantitative parameters of CEUS

For PTC ≤ 10 mm, there were no statistically significant differences between the groups CLNM (+) and CLNM (-) for all quantitative parameters of CEUS (*P* > 0.05). However, for PTC > 10 mm, the two groups differed significantly in terms of PI, MTT, and SL (*P* = 0.032, 0.031, and 0.007, respectively). There were no significant differences in TTP, AUC, AWI, or AWO (*P* > 0.05 for all) (Table 3, Figure 2).

3.4. Independent indicators correlated with CLNM

Multivariate analysis indicated that for PTC ≤ 10 mm, microcalcification (*P* = 0.001, OR = 4.165, 95% CI: 1.798 – 9.646) and multifocality (*P* = 0.031, OR = 2.540, 95% CI: 1.088 – 5.929) on CUS were independent indicators for predicting CLNM (Table 4). However, for

PTC > 10 mm, capsule contact (*P* = 0.015, OR = 4.401, 95% CI: 1.335 – 14.516) and multifocality (*P* = 0.021, OR = 4.233, 95% CI: 1.240 – 14.445) on CUS and PI (*P* = 0.021, OR = 5.898, 95% CI: 1.312 – 26.508) on CEUS were independent predictors of CLNM (Tables 4 and 5, respectively).

3.5. Predicting values of CLNM for PTC

For PTC ≤ 10 mm, the AUC for CUS (microcalcification combined with multifocality) was 0.716 with 87.500% sensitivity and 48.193% specificity (Table 6). For PTC > 10 mm, the AUC of PI was 0.703 with 92.308% sensitivity and 48.387% specificity by the cut-off of 5.8 dB, and the AUC of PI combined with CUS (capsule contact combined with multifocality) was 0.831 with 84.615% sensitivity and 74.193%, was significantly higher than that of PI and CUS (both *P* < 0.05) (Table 6). Figure 3 shows the ROC curves of capsule contact, multifocality, and PI correlated with CLNM.

4. Discussion

As CLNM is associated with the prognosis and treatment of PTC, correctly predicting CLNM is essential for PTC patients (*23-25*). CUS is generally the preferred choice for predicting CLNM in PTC because it is conveniently available, non-invasive, inexpensive, and high resolution. However, CUS may not always be reliable because of its overlap with CUS features associated with PTC with or without CLNM. In various studies, the risk factors of CUS for predicting CLNM have differed, including shape, size, boundary, multifocality, capsule contact, calcification, and blood flow (*26-30*). In the current study, we analyzed the CUS characteristics of PTC based on tumor size and calculated the prediction efficiency
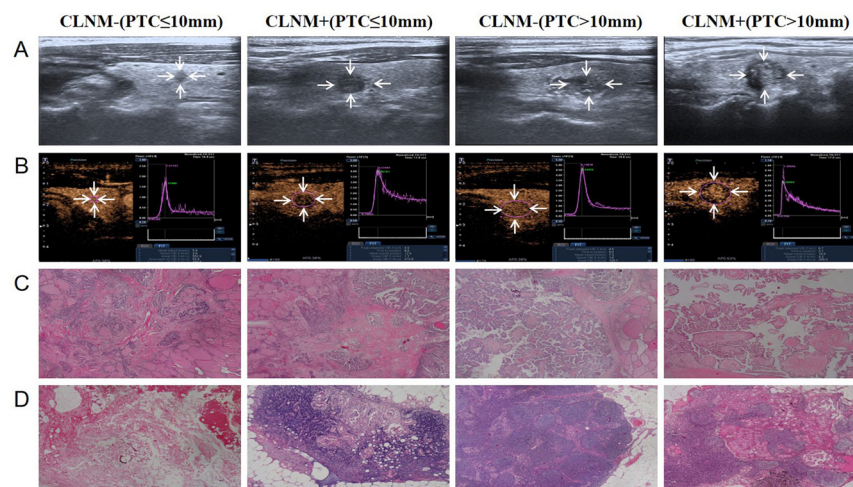
Figure 2. CUS, CEUS, pathology, and corresponding lymph node pathological images of PTC (≤ 10 mm and > 10 mm). **(A)** CUS feature of PTC (≤ 10 mm and > 10 mm) with or without CLNM. **(B)** The quantitative parameters of CEUS of PTC (≤ 10 mm and > 10mm) with or without CLNM. **(C)** Histopathology of PTC (≤ 10 mm and > 10 mm) with or without CLNM. **(D)** Histopathology of benign lymph nodes and metastatic lymph nodes in the neck (≤ 10 mm and > 10 mm). Above figures show that in PTC ≤ 10 mm, microcalcifications are more prone to cervical lymph node metastasis, while PTC > 10 mm, capsule contact and PI > 5.8 dB are more prone to lymph node metastasis.

Table 2. CUS features for PTC

Characteristics	≤ 10 mm (n = 123)		P	> 10 mm (n = 70)		P
	CLNM (-) (n = 83)	CLNM (+) (n = 40)		CLNM (-) (n = 31)	CLNM (+) (n = 39)	
Location			0.279			0.058
Lower	17 (13.8)	5 (4.1)		7 (10.0)	35 (50.0)	
Upper/middle	66 (53.6)	35 (28.5)		24 (34.3)	4 (5.7)	
Composition			0.148			1.000
Solid	83 (67.5)	39 (31.7)		30 (42.9)	38 (54.3)	
Mixed	0 (0)	1 (0.8)		1 (1.4)	1 (1.4)	
Echogenicity			0.377			0.287
hypoechoic	77 (62.6)	35 (28.5)		29 (41.4)	36 (51.4)	
Iso/hyperechoic	6 (4.9)	5 (4.1)		2 (2.9)	3 (4.3)	
Shape			0.085			0.095
Taller than wide	34 (27.6)	23 (18.7)		27 (38.6)	38 (54.3)	
Wider than tall	49 (39.8)	17 (13.8)		4 (5.7)	1 (1.4)	
Margin			0.514			0.024
Regular	32 (26.0)	13 (10.6)		17 (24.3)	11 (15.7)	
Irregular	51 (41.5)	27 (21.9)		14 (20.0)	28 (40.0)	
Microcalcification			0.000			0.250
Absent	51 (41.5)	11 (8.9)		17 (24.3)	16 (22.9)	
Present	32 (26.0)	29 (23.6)		14 (20.0)	23 (32.9)	
Halo sign			0.349			0.425
Absent	80 (65.0)	37 (30.1)		29 (41.4)	38 (54.3)	
Present	3 (2.4)	3 (2.4)		2 (2.9)	1 (1.4)	
Capsule contact			0.629			0.030
Absent	75 (61.0)	35 (28.5)		20 (28.6)	15 (21.4)	
Present	8 (6.5)	5 (4.1)		11 (15.7)	24 (34.3)	
Diffuse lesion			0.957			1.000
Absent	77 (62.6)	37 (30.1)		29 (41.4)	37 (52.9)	
Present	6 (4.9)	3 (2.4)		2 (2.9)	2 (2.9)	
Multifocal			0.019			0.037
Absent	63 (51.2)	22 (17.9)		22 (31.4)	18 (25.7)	
Present	20 (16.3)	18 (14.6)		9 (12.9)	21 (30.0)	
CDFI patterns			0.199			0.512
Avascularity	56 (45.5)	23 (18.7)		8 (11.4)	6 (8.6)	
Central	16 (13.0)	6 (4.9)		5 (7.1)	7 (10.0)	
Peripheral	5 (4.1)	3 (2.4)		6 (8.6)	5 (7.1)	
Mixed	6 (4.9)	8 (6.5)		12 (17.1)	21 (30.0)	

CDFI, color Doppler flow imaging; CUS, conventional ultrasound; CLNM, cervical lymph node metastasis; PTC, papillary thyroid carcinoma; Values are presented as the number (%).

Table 3. Quantitative parameters of CEUS for PTC

Characteristics	≤ 10 mm (n = 123)		P	> 10 mm (n = 70)		P
	CLNM (-) (n = 83)	CLNM (+) (n = 40)		CLNM (-) (n = 31)	CLNM (+) (n = 39)	
PI (dB)	14.8 ± 19.6	11.9 ± 9.7	0.389	12.5 ± 13.1	25.3 ± 33.2	0.032
TTP (s)	7.6 ± 6.9	12.5 ± 26.1	0.215	5.9 ± 3.6	4.6 ± 1.9	0.053
MTT (s)	40.8 ± 57.8	40.3 ± 60.3	0.965	53.9 ± 67.3	23.2 ± 41.4	0.031
SL (dB / s)	7.1 ± 26.1	4.1 ± 4.7	0.467	2.9 ± 2.9	8.2 ± 10.9	0.007
AUC (dB · s)	716.6 ± 875.9	638.2 ± 646.7	0.416	864.7 ± 1312.5	1037.2 ± 1224.4	0.573
AWI (dB · s)	42.5 ± 55.9	67.4 ± 176.4	0.244	50.7 ± 79.9	66.3 ± 84.9	0.435
AWO (dB · s)	676.5 ± 822.9	585.4 ± 612.6	0.535	814.1 ± 1234.5	970.7 ± 1141.6	0.484

AUC, area under the receiver operating characteristic curve; AWI, area wash in; AWO, area wash out; CEUS, contrast-enhanced ultrasound; CLNM, cervical lymph node metastasis; MTT, mean transit time; PTC, papillary thyroid carcinoma; PI, peak intensity; TTP, time to peak; SL, slope. Values are presented as the number (%).

of CLNM. We confirmed that microcalcification and multifocality on CUS are related to CLNM in nodules ≤ 10 mm. For nodules > 10 mm in size, capsule contact and multifocality on CUS were independent predictors of CLNM. The results of the present study show that CLNM is strongly related to multifocality, whether the nodule is ≤ 10 mm or > 10 mm. These findings are in line with previous reports, which documented

Table 4. Multivariate analysis of CUS characteristics associated with CLNM in PTC

Independent risk factor	β	S.E.	Wald	df	*P*	OR	95% CI
≤ 10 mm PTC							
Microcalcification	1.427	0.428	11.085	1	0.001	4.165	1.798 - 9.646
Multifocal	0.932	0.432	4.648	1	0.031	2.540	1.088 - 5.929
Constant	-1.846	0.379	23.780	1	0.000	0.158	/
> 10 mm PTC							
Margin	0.717	0.547	1.719	1	0.190	2.047	0.701 - 5.976
Capsule contact	1.482	0.609	5.924	1	0.015	4.401	1.335 - 14.516
Multifocal	1.443	0.626	5.309	1	0.021	4.233	1.240 - 14.445
Constant	-1.496	0.579	6.678	1	0.010	0.224	/

CI, confidence interval; CUS, conventional ultrasound; CLNM, cervical lymph node metastasis; df, degrees of freedom; OR, odds ratio; PTC, papillary thyroid carcinoma; S.E., standard error.

**Table 5. Multivariate analysis of quantitative parameters of CEUS associated with CLNM in PTC (> 10 mm)**

Independent risk factor	β	S.E.	Wald	df	*P*	OR	95% CI
PI	1.775	0.767	5.356	1	0.021	5.898	1.312 - 26.508
MTT	1.314	0.779	2.842	1	0.092	3.720	0.808 - 17.129
SL	0.727	0.652	1.243	1	0.265	2.069	0.576 - 7.429
Constant	-2.048	0.854	7.945	1	0.005	0.090	/

CEUS, contrast-enhanced ultrasound; CLNM, cervical lymph node metastasis; df, degrees of freedom; MTT, mean transit time; OR, odds ratio; PTC, papillary thyroid carcinoma; PI, peak intensity; S.E., standard error; SL, slope.

Table 6. ROC analysis for predicting CLNM in PTC

Independent risk factor	Cut-off value	Sensitivity	Specificity	AUC (95% CI)
≤ 10 mm PTC				
Multifocal[1]	Present	18 / 40 (45.0)	63 / 83 (75.9)	0.605 (0.512 - 0.961)
Microcalcification[2]	Present	29 / 40 (72.5)	51 / 83 (61.4)	0.670 (0.579 - 0.752)
1 + 2	1 + 2	35 / 40 (87.5)	40 / 83 (48.2)	0.716 (0.628 - 0.794)
> 10 mm PTC				
Capsule contact[3]	Present	24 / 39 (61.5)	20 / 31 (64.5)	0.630 (0.506 - 0.743)
Multifocal[4]	Present	21 / 39 (53.8)	22 / 31 (70.9)	0.624 (0.500 - 0.737)
3 + 4	3 + 4	36 / 39 (92.3)	13 / 31 (41.9)	0.707 (0.586 - 0.810)
PI[5]	5.8	36 / 39 (92.3)	15 / 31 (48.4)	0.703 (0.582 - 0.807)
3 + 4 + 5	3 + 4 + 5	33 / 39 (84.6)	23 / 31 (74.2)	0.831 (0.722 - 0.910)

AUC, area under the receiver operating characteristic curve; CLNM, cervical lymph node metastasis; PTC, papillary thyroid carcinoma; PI, peak intensity; ROC, receiver operating characteristic. Values are presented as the number (%).
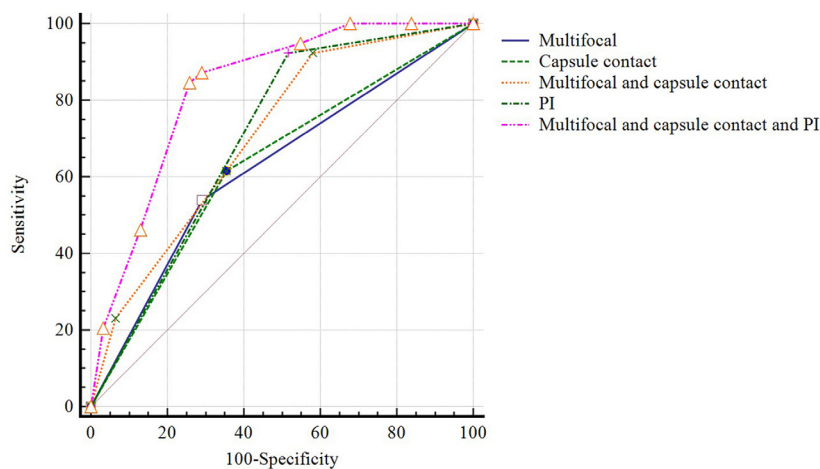
Figure 3. ROC analysis for the features of CUS and quantitative parameters of CEUS in predicting CLNM in patients with PTCs (> 10 mm). The ROC curves of capsule contact, multifocality and PI correlating with CLNM.

that multifocality in PTC is associated with metastatic spread in histopathology (*31,32*). The difference in the results between nodules ≤ 10 and > 10 mm may be due to tumor growth and metabolism. Microcalcification is a malignant feature of CUS. In histopathology, microcalcification in PTC is mainly caused by psammoma bodies with a diameter of 10-100 μm and may be related to the aggressive behavior of PTC (*33*). Owing to other pathological structures, such as focal fibrosis in nodules > 10 mm, distinguishing fibrosis from microcalcification is difficult (*34*). Capsule contact was identified as a risk factor for CLNM in nodules measuring > 10 mm, probably because cancer cells are easily destroyed by the capsule and spread to other parts, such as fat, muscle, and lymphoid tissue (*32*). Though CUS had a high sensitivity in the prediction of CLNM for PTC ≤ 10 mm and PTC > 10 mm (87.5%, 92.3%, respectively), it showed a low specificity for that (48.2%, 41.9%, respectively). Therefore, further imaging studies are required to predict cervical lymph node metastasis in patients with PTC.

Presently, CEUS is a topic of active research in ultrasound medicine. This modality can detect both large-diameter vessels and high-velocity blood flow, significantly improving the detection of small vessels within a lesion (*35-37*). Furthermore, CEUS offers advantages over other imaging techniques such as CT and MRI, including the ability for repeated examinations, the absence of radiation exposure, no hepatorenal toxicity, and a low risk of allergic reactions. Previous studies have identified the usefulness of CEUS for predicting CLNM in PTC (*38-40*). However, most of these studies focused on the qualitative analysis of CEUS features (*41,42*). The fact that qualitative analysis based on visual observation is subjective and may not provide an objective evaluation of the details of PTC perfusion is worth noting. In contrast, quantitative CEUS can provide objective perfusion characteristics with exceedingly good reproducibility, reduce sonographic dependency and subjective errors, and provide steady and reliable results.

Several studies have confirmed that microvascular density correlates with CLNM in PTC (*43,44*). A higher microvascular density in the tumor tissue is associated with a higher likelihood of CLNM (*45*). Microvascular density is considered the "gold standard" to quantitatively evaluate the formation of tumor neovascularization, but it requires invasive procedures such as surgery or puncture to obtain tissue specimens (*46*). Fortunately, time-intensity curve (TIC) parameters derived from CEUS reflect the process of intensity enhancement in the region of interest (ROI) over time following contrast agent injection. These quantitative parameters of CEUS provide an objective reflection of tissue microcirculation changes, making it a non-invasive alternative for assessing neovascularization and predicting CLNM in PTC. PI positively correlated with microvascular density and was defined as the intensity

at which the contrast agent reached peak perfusion. The results of this study indicated that for >10 mm PTC, the difference in PI between the CLNM (+) and CLNM (-) groups was statistically significant (25.30 ± 33.17 *vs.* 12.50 ± 13.10 dB, *P* = 0.032). Further, the multifactor analysis suggested that PI was a predictive factor for CLNM, which is in agreement with earlier findings (*47,48*). The slope is defined as the rate at which the contrast agent reaches its peak intensity. Because of the larger new capillaries in the tumor, a larger amount of contrast agent centralizes in the PTC, resulting in a steeper slope. The slope of PTC > 10 mm with CLNM was higher than that of PTC > 10 mm without CLNM. The MTT reflects the retention time of the contrast agent in the ROI, which is closely related to the blood flow velocity. Wei *et al.* (*49*) reported that the internal blood vessels of malignant tumors are thicker than those of benign nodules and that arteriovenous fistulas are easy to form, which shortens the retention time of contrast agents in the blood vessels (*50*). The present study found that the MTT of PTC > 10 mm in the CLNM (+) group was shorter than the CLNM (-) group. However, the results of multivariate analysis suggested that SL and MTT were not associated with CLNM for PTC > 10 mm (*P* > 0.05). All quantitative parameters of CEUS in PTC ≤ 10 mm were not statistically different between the two groups (*P* > 0.05). The finding may be due to the fact that small tumor neovascularization beds in PTC ≤ 10 mm are not sufficiently developed; insufficient number and small diameter result in less perfusion of contrast agent. Further, owing to the inevitable breathing and tension movements of patients, the dynamic ROI image of nodules ≤ 10 mm is often unstable. Because the lesion is quite small, a slight movement will cause a deviation in the parameters from the ROI. Thus, accurate tracking and identification of small lesions are difficult. Consequently, the quantitative parameters obtained after analysis may have been inaccurate, which could explain why these parameters did not show any differences. Therefore, we consider that the use of quantitative CEUS in nodules ≤ 10 mm to predict CLNM is limited.

Furthermore, in our study, we calculated and compared the AUC for predicting CLNM in PTC using the quantitative parameters of CEUS, CUS, and a combination of both. For nodules ≤ 10 mm, the AUC for CUS features in predicting CLNM was 0.716, which was higher than the AUC of 0.687 reported by Luo *et al.* (*51*). The AUCs for CUS and CEUS in predicting CLNM in nodules > 10 mm were 0.706 and 0.703, respectively. Additionally, our study demonstrated that the AUC for the combination of CUS and CEUS was 0.831, which was significantly higher than that for CUS alone (*P* < 0.05). These findings suggest that the combination of CUS and CEUS can improve the predictive accuracy of CLNM, particularly for nodules larger than 10 mm.

Acknowledging the limitations of this study is important. First, this being a single-center study, a

selection bias may have been introduced. Therefore, large-scale, multicenter studies are necessary to validate these results. Second, although quantitative evaluation of CEUS is considered more objective than qualitative evaluation, it requires skilled operators and thus may be less flexible. Even a slight movement of the ROI in a target lesion can lead to inaccurate results. Standardization of the technique and further training of operators may be necessary to improve accuracy. Third, the study did not survey the factors related to long-term survival or locoregional recurrence rates. Future research should address these questions to provide a deeper understanding of the topic.

In conclusion, this study found that certain characteristics, such as microcalcification and multifocality, observed in CUS are helpful in predicting CLNM in nodules that are 10 mm or smaller. However, the use of quantitative CEUS to predict lymph node metastasis in smaller nodules is limited. For nodules larger than 10 mm, characteristics such as capsule contact, multifocality observed on CUS, and peak intensity observed on CEUS can be used to predict CLNM. Quantitative parameters obtained from CEUS are valuable for evaluating CLNM. The combination of CUS and CEUS can be an effective approach for predicting CLNM in nodules larger than 10 mm.

Conflict of Interest: The authors have no conflicts of interest to disclose.

References

1. Colonna M, Uhry Z, Guizard AV, Delafosse P, Schvartz C, Belot A, Grosclaude P; FRANCIM network. Recent trends in incidence, geographical distribution, and survival of papillary thyroid cancer in France. Cancer Epidemiol. 2015; 39:511-518.
2. Al-Brahim N, Asa SL. Papillary thyroid carcinoma: An overview. Arch Pathol Lab Med. 2006; 130:1057-1062.
3. Pellegriti G, Frasca F, Regalbuto C, Squatrito S, Vigneri R. Worldwide increasing incidence of thyroid cancer: Update on epidemiology and risk factors. J Cancer Epidemiol. 2013; 2013:965212.
4. Sipos JA. Advances in ultrasound for the diagnosis and management of thyroid cancer. Thyroid. 2009; 19:1363-1372.
5. Baek SK, Jung KY, Kang SM, Kwon SY, Woo JS, Cho SH, Chung EJ. Clinical risk factors associated with cervical lymph node recurrence in papillary thyroid carcinoma. Thyroid. 2010; 20:147-152.
6. Xu S, Yao J, Zhou W, Chen L, Zhan W. Clinical characteristics and ultrasonographic features for predicting central lymph node metastasis in clinically node-negative papillary thyroid carcinoma without capsule invasion. Head Neck. 2019; 41:3984-3991.
7. Zhang L, Yang J, Sun Q, Liu Y, Liang F, Liu Z, Chen G,

Chen S, Shang Z, Li Y, Li X. Risk factors for lymph node metastasis in papillary thyroid microcarcinoma: older patients with fewer lymph node metastases. Eur J Surg Oncol. 2016; 42:1478-1482.
8. Machens A, Hauptmann S, Dralle H. Lymph node dissection in the lateral neck for completion in central node-positive papillary thyroid cancer. Surgery. 2009; 145:176-181.
9. Haugen BR, Alexander EK, Bible KC, *et al.* 2015 American thyroid association management guidelines for adult patients with thyroid nodules and differentiated thyroid cancer: the American thyroid association guidelines task force on thyroid nodules and differentiated thyroid cancer. Thyroid. 2016; 26:1-133.
10. Liu C, Xiao C, Chen J, Li X, Feng Z, Gao Q, Liu Z. Risk factor analysis for predicting cervical lymph node metastasis in papillary thyroid carcinoma: a study of 966 patients. BMC Cancer. 2019; 19:622.
11. Viola D, Materazzi G, Valerio L, *et al*. Prophylactic central compartment lymph node dissection in papillary thyroid carcinoma: Clinical implications derived from the first prospective randomized controlled single institution study. J Clin Endocrinol Metab. 2015; 100:1316-1324.
12. Zhao WJ, Luo H, Zhou YM, Dai WY, Zhu JQ. Evaluating the effectiveness of prophylactic central neck dissection with total thyroidectomy for cN0 papillary thyroid carcinoma: An updated meta-analysis. Eur J Surg Oncol. 2017; 43:1989-2000.
13. Zhao C, Jiang W, Gao Y, Niu W, Zhang X, Xin L. Risk factors for lymph node metastasis (LNM) in patients with papillary thyroid microcarcinoma (PTMC): role of preoperative ultrasound. J Int Med Res. 2017; 45:1221-1230.
14. Jin WX, Ye DR, Sun YH, Zhou XF, Wang OC, Zhang XH, Cai YF. Prediction of central lymph node metastasis in papillary thyroid microcarcinoma according to clinicopathologic factors and thyroid nodule sonographic features: a case-control study. Cancer Manag Res. 2018; 10:3237-3243.
15. Li J, Liu J, Qian L. Suspicious ultrasound characteristics correlate with multiple factors that predict central lymph node metastasis of papillary thyroid carcinoma: Significant role of HBME-1. Eur J Radiol. 2020; 123:108801.
16. Chen J, Li XL, Zhang YF, Wang D, Wang Q, Zhao CK, Li MX, Wei Q, Ji G, Xu HX. Ultrasound validation of predictive model for central cervical lymph node metastasis in papillary thyroid cancer on BRAF. Future Oncol. 2020; 16:1607-1618.
17. Kouvaraki MA, Shapiro SE, Fornage BD, Edeiken-Monro BS, Sherman SI, Vassilopoulou-Sellin R, Lee JE, Evans DB. Role of preoperative ultrasonography in the surgical management of patients with thyroid cancer. Surgery. 2003; 134:946-954.
18. Chen M, Zhang K, Xu Y, Zhang S, Cao Y, Sun W. Shear wave elastography and contrast-enhanced ultrasonography in the diagnosis of thyroid malignant nodules. Mol Clin Oncol. 2016; 5:724-730.
19. Trimboli P, Castellana M, Virili C, Havre RF, Bini F, Marinozzi F, D'Ambrosio F, Giorgino F, Giovanella L, Prosch H, Grani G, Radzina M, Cantisani V. Performance of contrast-enhanced ultrasound (CEUS) in assessing thyroid nodules: A systematic review and meta-analysis using histological standard of reference. Radiol Med. 2020; 125:406-415.
20. Xu Y, Qi X, Zhao X, Ren W, Ding W. Clinical diagnostic

value of contrast-enhanced ultrasound and TI-RADS classification for benign and malignant thyroid tumors: One comparative cohort study. Medicine (Baltimore). 2019; 98:e14051.

21. Deng J, Zhou P, Tian S, Zhang L, Li J, Qian Y. Comparison of diagnostic efficacy of contrast-enhanced ultrasound, acoustic radiation force impulse imaging, and their combined use in differentiating focal solid thyroid nodules. PLoS One. 2014; 9:e90674.

22. Liu Q, Cheng J, Li J, Gao X, Li H. The diagnostic accuracy of contrast-enhanced ultrasound for the differentiation of benign and malignant thyroid nodules: A PRISMA compliant meta-analysis. Medicine (Baltimore). 2018; 97:e13325.

23. Ito Y, Fukushima M, Higashiyama T, Kihara M, Takamura Y, Kobayashi K, Miya A, Miyauchi A. Tumor size is the strongest predictor of microscopic lymph node metastasis and lymph node recurrence of N0 papillary thyroid carcinoma. Endocr J. 2013; 60:113-117.

24. Liu W, Cheng R, Su Y, Diao C, Qian J, Zhang J, Ma Y, Fan Y. Risk factors of central lymph node metastasis of papillary thyroid carcinoma: A single-center retrospective analysis of 3273 cases. Medicine (Baltimore). 2017; 96:e8365.

25. Perrier ND, Brierley JD, Tuttle RM. Differentiated and anaplastic thyroid carcinoma: Major changes in the American Joint Committee on Cancer eighth edition cancer staging manual. CA Cancer J Clin. 2018; 68:55-63.

26. Yao X, Meng Y, Guo R, Lu G, Jin L, Wang Y, Yang D. Value of ultrasound combined with immunohistochemistry evaluation of central lymph node metastasis for the prognosis of papillary thyroid carcinoma. Cancer Manag Res. 2020; 12:8787-8799.

27. Huang C, Cong S, Liang T, Feng Z, Gan K, Zhou R, Guo Y, Luo S, Liang K, Wang Q. Development and validation of an ultrasound-based nomogram for preoperative prediction of cervical central lymph node metastasis in papillary thyroid carcinoma. Gland Surg. 2020; 9:956-967.

28. Ji WL, Ya HL, Kai L, Bo H, Yue JZ, Hao TW, Tao Y. Clinicopathologic factors and preoperative ultrasonographic characteristics for predicting central lymph node metastasis in papillary thyroid microcarcinoma: A single center retrospective study. Braz J Otorhinolaryngol. 2022; 88:36-45.

29. Luo X, Wang J, Xu M, Zou X, Lin Q, Zheng W, Guo Z, Li A, Han F. Risk model and risk stratification to preoperatively predict central lymph node metastasis in papillary thyroid carcinoma. Gland Surg. 2020; 9:300-310.

30. Guo L, Ma YQ, Yao Y, Wu M, Deng ZH, Zhu FW, Luo YK, Tang J. Role of ultrasonographic features and quantified BRAFV600E mutation in lymph node metastasis in Chinese patients with papillary thyroid carcinoma. Sci Rep. 2019; 9:75.

31. Chen BD, Zhang Z, Wang KK, Shang MY, Zhao SS, Ding WB, Du R, Yu Z, Xu XM. A multivariable model of BRAFV600E and ultrasonographic features for predicting the risk of central lymph node metastasis in cN0 papillary thyroid microcarcinoma. Cancer Manag Res. 2019; 11:7211-7217.

32. Xu JM, Xu HX, Li XL, Bo XW, Xu XH, Zhang YF, Guo LH, Liu LN, Qu S. A risk model for predicting central lymph node metastasis of papillary thyroid microcarcinoma including conventional ultrasound and acoustic radiation force impulse elastography. Medicine (Baltimore). 2016; 95:e2558.

33. Das DK, Sheikh ZA, George SS, Al-Baquer T, Francis IM. Papillary thyroid carcinoma: Evidence for intracytoplasmic formation of precursor substance for calcification and its release from well-preserved neoplastic cells. Diagn Cytopathol. 2008; 36:809-812.

34. Feng JW, Hong LZ, Wang F, Wu WX, Hu J, Liu SY, Jiang Y, Ye J. A nomogram based on clinical and ultrasound characteristics to predict central lymph node metastasis of papillary thyroid carcinoma. Front Endocrinol (Lausanne). 2021; 12:666315.

35. Sidhu P, Cantisani V, Dietrich C, *et al*. The EFSUMB guidelines and recommendations for the clinical practice of contrast-enhanced ultrasound (CEUS) in non-hepatic applications: update 2017 (Short Version). Ultraschall Med. 2018; 39:154-180.

36. Ma J, Wang Y, Xi X, Tang J, Wang L, Wang L, Wang D, Liang X, Zhang B. Contrast-enhanced ultrasound combined targeted microbubbles for diagnosis of highly aggressive papillary thyroid carcinoma. Front Endocrinol (Lausanne). 2023; 14:1052862.

37. Wilsen CB, Patel MK, Douek ML, Masamed R, Dittmar KM, Lu DSK, Raman SS. Contrast-enhanced ultrasound for abdominal image-guided procedures. Abdom Radiol (NY). 2023; 48:1438-1453.

38. Yu Y, Shi LL, Zhang HW, Wang Q. Performance of contrast-enhanced ultrasound for lymph node metastasis in papillary thyroid carcinoma: A meta-analysis. Endocr Connect. 2023; 12:e220341.

39. Li QL, Ma T, Wang ZJ, Huang L, Liu W, Chen M, Sang T, Ren XG, Tong J, Cao CL, Dong J, Li J. The value of contrast-enhanced ultrasound for the diagnosis of metastatic cervical lymph nodes of papillary thyroid carcinoma: A systematic review and meta-analysis. J Clin Ultrasound. 2022; 50:60-69.

40. Fang F, Gong Y, Liao L, Ye F, Zuo Z, Li X, Zhang Q, Tang K, Xu Y, Zhang R, Chen S, Niu C. Value of contrast-enhanced ultrasound for evaluation of cervical lymph node metastasis in papillary thyroid carcinoma. Front Endocrinol (Lausanne). 2022; 13:812475.

41. Zhan J, Diao X, Chen Y, Wang W, Ding H. Predicting cervical lymph node metastasis in patients with papillary thyroid cancer (PTC) - Why contrast-enhanced ultrasound (CEUS) was performed before thyroidectomy. Clin Hemorheol Microcirc. 2019; 72:61-73.

42. Zhan J, Zhang LH, Yu Q, Li CL, Chen Y, Wang WP, Ding H. Prediction of cervical lymph node metastasis with contrast-enhanced ultrasound and association between presence of BRAF(V600E) and extrathyroidal extension in papillary thyroid carcinoma. Ther Adv Med Oncol. 2020; 12:1758835920942367.

43. Liu Z, Li C. Correlation of lymph node metastasis with contrast-enhanced ultrasound features, microvessel density and microvessel area in patients with papillary thyroid carcinoma. Clin Hemorheol Microcirc. 2022; 82:361-370.

44. Perivoliotis K, Samara AA, Koutoukoglou P, Ntellas P, Dadouli K, Sotiriou S, Ioannou M, Tepetes K. Microvessel density in differentiated thyroid carcinoma: A systematic review and meta-analysis. World J Methodol. 2022; 12:448-458.

45. Zhan W, Zhou P, Zhou J, Xu S, Chen K. Differences in sonographic features of papillary thyroid carcinoma between neck lymph node metastatic and nonmetastatic groups. J Ultrasound Med. 2012; 31:915-920.

46. Mori N, Mugikura S, Takahashi S, Ito K, Takasawa

C, Li L, Miyashita M, Kasajima A, Mori Y, Ishida T, Kodama T, Takase K. Quantitative analysis of contrast-enhanced ultrasound imaging in invasive breast cancer: A novel technique to obtain histopathologic information of microvessel density. Ultrasound Med Biol. 2017; 43:607-614.

47. Liu Y, Zhou H, Yang P, Zhou Y, Wu J, Chen C, Ye M, Luo J. Contrast-enhanced ultrasonography features of papillary thyroid carcinoma for predicting cervical lymph node metastasis. Exp Ther Med. 2017; 14:4321-4327.

48. Tao L, Zhou W, Zhan W, Li W, Wang Y, Fan J. Preoperative prediction of cervical lymph node metastasis in papillary thyroid carcinoma *via* conventional and contrast-enhanced ultrasound. J Ultrasound Med. 2020; 39:2071-2080.

49. Wei S, Fu N, Yao C, Liu P, Yang B. Two-and three-dimensional contrast-enhanced sonography for assessment of renal tumor vasculature: preliminary observations. J Ultrasound Med. 2013; 32:429-437.

50. Strouthos C, Lampaskis M, Sboros V, Mcneilly A, Averkiou M. Indicator dilution models for the quantification of microvascular blood flow with bolus administration of ultrasound contrast agents. IEEE Trans Ultrason Ferroelectr Freq Control. 2010; 57:1296-1310.

51. Luo Y, Zhao Y, Chen K, Shen J, Shi J, Lu S, Lei J, Li Z, Luo D. Clinical analysis of cervical lymph node metastasis risk factors in patients with papillary thyroid microcarcinoma. J Endocrinol Invest. 2019; 42:227-236.

§These authors contributed equally to this work.
Address correspondence to:
Ling Wang, Laboratory for Reproductive Immunology, Obstetrics and Gynecology Hospital of Fudan University, 419 Fangxie Road, Shanghai, China 200011.
E-mail: Dr.wangling@fudan.edu.cn

Lin Chen, Department of Ultrasound, Huadong Hospital of Fudan University, 211 West Yan'an Rd, Shanghai, China 200040.
E-mail: cl_point@126.com